

Supporting Information for

**Enhanced enzymatic activity exerted by a packed
assembly of single type of enzyme**

Huyen Dinh, Eiji Nakata, Kaori Mutsuda-Zapater, Masayuki Saimura, Masahiro Kinoshita,
Takashi Morii*

* Corresponding author. Email: t-morii@iae.kyoto-u.ac.jp

This file includes:

- **Table S1**
- **Figure S1-S17**
- **References**

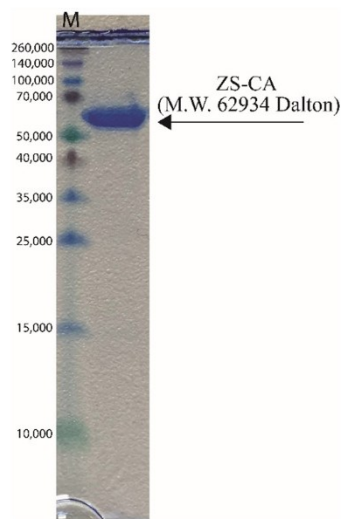
SUPPLEMENTARY TABLE

Table S1 List of primers used in this study

Primers	Sequences (from 5' to 3')
F_HCAII	CCAGCGCGACCATGTCCCATCACTGGGGGTAC
R_HCAII	GCACCAACCAGCCACAGCAGTTGTGTCAAGC
F_SNAP_Kpn_HCAII	GGTTAATGGTACCGGAGGCATGTCCCATCACTGGGGGTACGGCAAACACAACGG
R_HCAII_Histag_NotI_	GGGAGCCTCTCGGAACTAACCCCTTTGAAGGAAGCTTTGATTTGCCTG
P1	
R_HCAII_Histag_NotI_	TATAATTTATATGCGGCCGCTTAATGATGATGATGATGGTGGGAGCCTCTCGGAACTA
P2	ACCC
F_NdeI_Zif268	ATATACATATGATGAAAACCGGGGAGAAAACGCCCCG
F-NdeI-HCA2	ATAATATAATCATATGATGTCCCATCACTGGGGGTACGGCAAACACAACGG

SUPPLEMENTARY FIGURES

a



b

```

MMKTGEKRPY ACPVESCDRR FSRSEDELTRH IRIHTGQKPF QCRICMRNFS RSDHLTTHIR
THTGEKPFAC DICGRKFARS DERKRHTKIH TGEKEFGGSG GSDKDCEMKR TTLDSPLGKL
ELSGCEQGLH EIKLLGKGTS AADAVEVPAP AAVLGGPEPL MQATAWLNAY FHQPEAIEEF
PVPALHHPVF QQESFTRQVL WKLLKVVKFG EVISYQQLAA LAGNPAATAA VKTALSGNPV
PILIPCHRUV SSSGAVGGYE GGLAVKEWLL AHEGHRGKLP GLGPAGGSPG LEVNGTGGMS
HHWGYGKHNG PEHWHKDFPI AKGERQSPVD IDTHTAKYDP SLKPLSVSYD QATSLRILNN
GHAFNVEFDD SQDKAVLKGG PLDGTYRLIQ FHFHWGSLDG QGSEHTVDKK KYAAELHLVH
WNTKYGDFGK AVQQPDGLAV LGIFLKVGS A KPGLOKVVDV LDSIKTKGKS ADFTNFDPRG
LLPESLDYWT YPGSLTTPPL LECVTWIVLK EPISVSSEQV LKFRKLNFG EGEPEELMVD
NWRPAQPLKN RQIKASFKGL VPRGSHHHHH H
  
```

Figure S1. (a) SDS-PAGE analysis of ZS-CA after purification. Lane M: molecular weight ladder (M.W. 10,000 – 260,000 Dalton). ZS-CA with molecular weight of 62,934 Dalton and the purity >95%. (b) Amino acid sequence of ZS-CA.

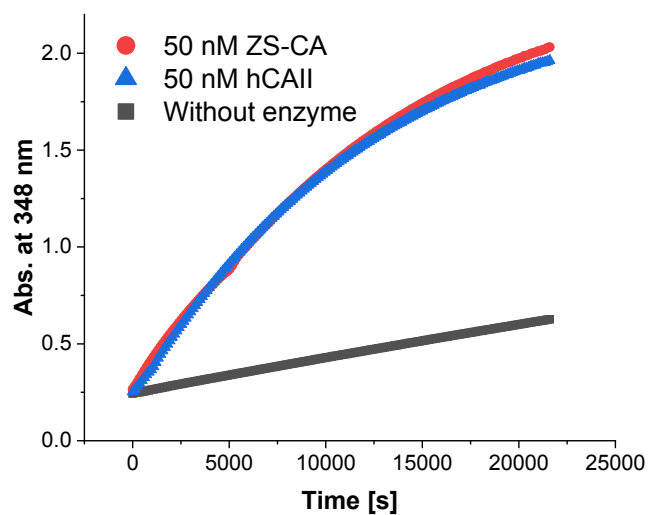


Figure S2. Comparison of the activity of ZS-CA and wild type hCAII. Time course changes for the reaction of *p*-NPA hydrolysis monitored at 348 nm were shown. The genetic fusion of hCAII to the modular adaptor ZS did not affect to the enzymatic activity. Reaction conditions: 50 nM ZS-CA or hCAII, 1 mM *p*-NPA in a buffer (pH 7.6) containing 50 mM HEPES, 12.5 mM MgCl₂, 1% acetonitrile, 1 μM ZnCl₂ and 0.001% Tween-20.

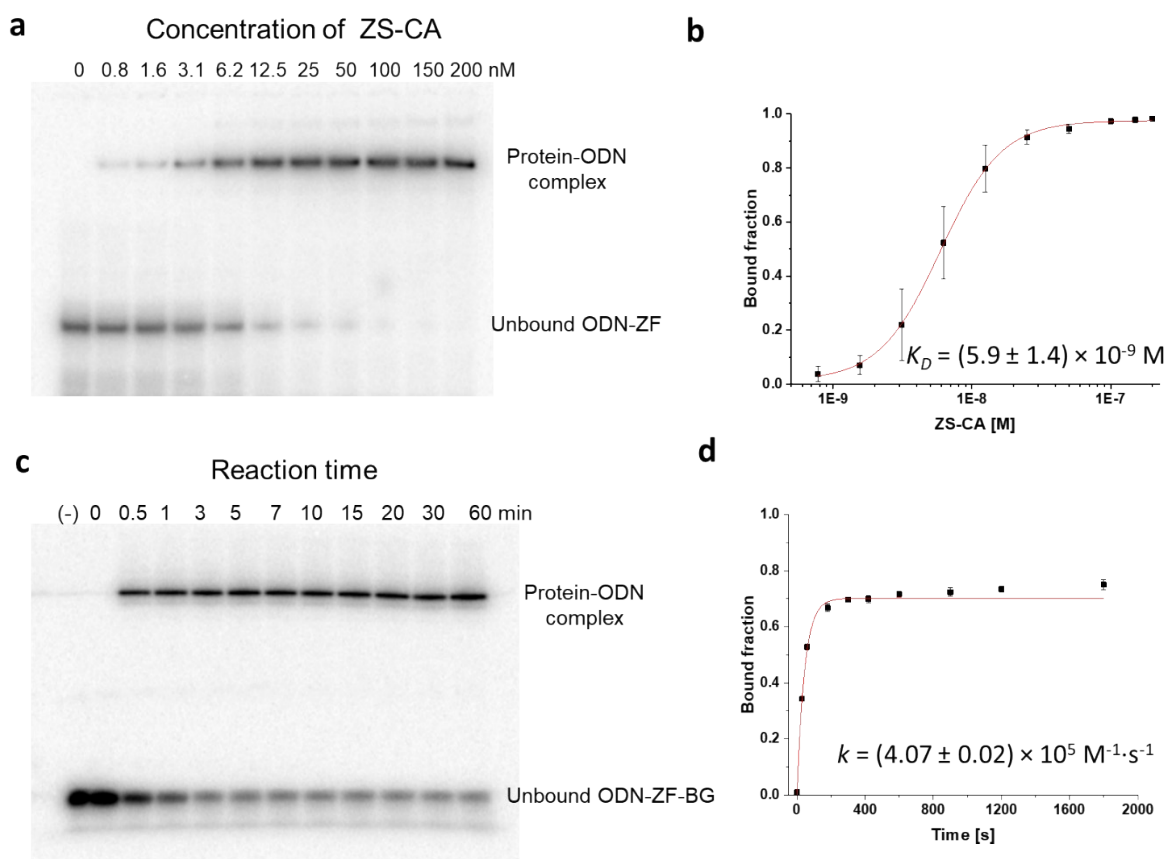


Figure S3. (a) An autoradiogram shows electrophoretic mobility shift titration of ZS-CA to 5'-³²P-labelled ODN-ZF in a buffer (pH 8.0) containing 40 mM Tris-HCl, 20 mM acetic acid, 12.5 mM MgCl₂, 5 mM β-mercaptomethanol, 1 μM ZnCl₂, 0.02% Tween-20, and 1 μg/ml BSA, at ambient temperature. (b) A semilogarithmic plot shows the fractions of 5'-³²P-labeled ODN-ZF bound to ZS-CA, with a fitting curve to obtain the equilibrium dissociation constant for the complexes of ZS-CA with ODN-ZF as $K_D = (5.9 \pm 1.4) \times 10^{-9} \text{ M}$.

The sequence of ODN-ZF:

5'-CGCGTATAACGCCACGCGGTTTCCGCGTGGGCGTTATACGC-3'

(c) An autoradiogram shows PAGE analysis of the crosslinking reactions of 5'-³²P-end-labeled ODN-ZF-BG (0.5 nM) with ZS-CA (10 nM) in a buffer (pH 8.0) containing 40 mM Tris-HCl, 20 mM acetic acid, 12.5 mM MgCl₂, 5 mM β-mercaptomethanol, 1 μM ZnCl₂, 0.02% Tween 20, and 1 μg/ml BSA, at ambient temperature. (d) A time-course profile for the crosslinking reaction of ODN-ZF-BG and ZS-CA to obtain the kinetic constant $k = (4.7 \pm 0.02) \times 10^5 \text{ M}^{-1} \cdot \text{s}^{-1}$.

The sequence of ODN-ZF-BG:

5'-CGCGTATAACGCCACGCGGTT^{BG}TCCGCGTGGGCGTTATACGC-3'

(T^{BG} = BG modified T, see Fig. 1c)

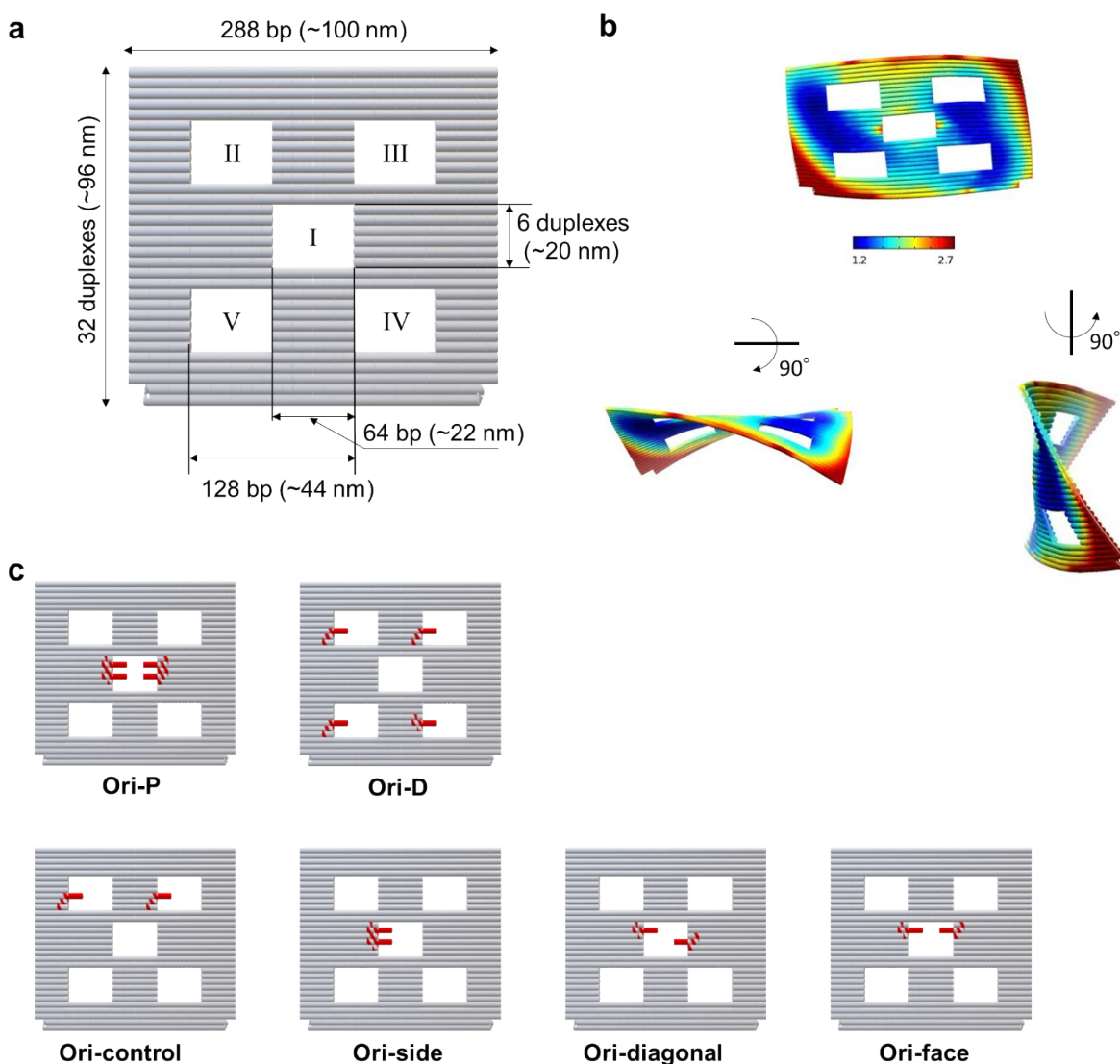


Figure S4. Illustrations show the structures of DNA origami scaffolds used in this study. (a) An illustration of DNA scaffold with five cavities. (b) Atomic models of predicted 3D solution shape of the DNA scaffold in three orthogonal views generated from CANDO simulation¹ with heat map color range for RMSF (Root-mean-square fluctuation): blue and red represent low and high relative flexibility, respectively. 0% (minimum) RMSF (bluest) = 1.172261 nm, 95% RMSF (reddest) = 2.746728 nm, maximum RMSF = 4.073864 nm. (c) The DNA scaffolds used in this study with 4 binding sites per scaffold: Ori-P and Ori-D; with 2 binding sites per scaffold: Ori-control, Ori-side, Ori-diagonal and Ori-face.

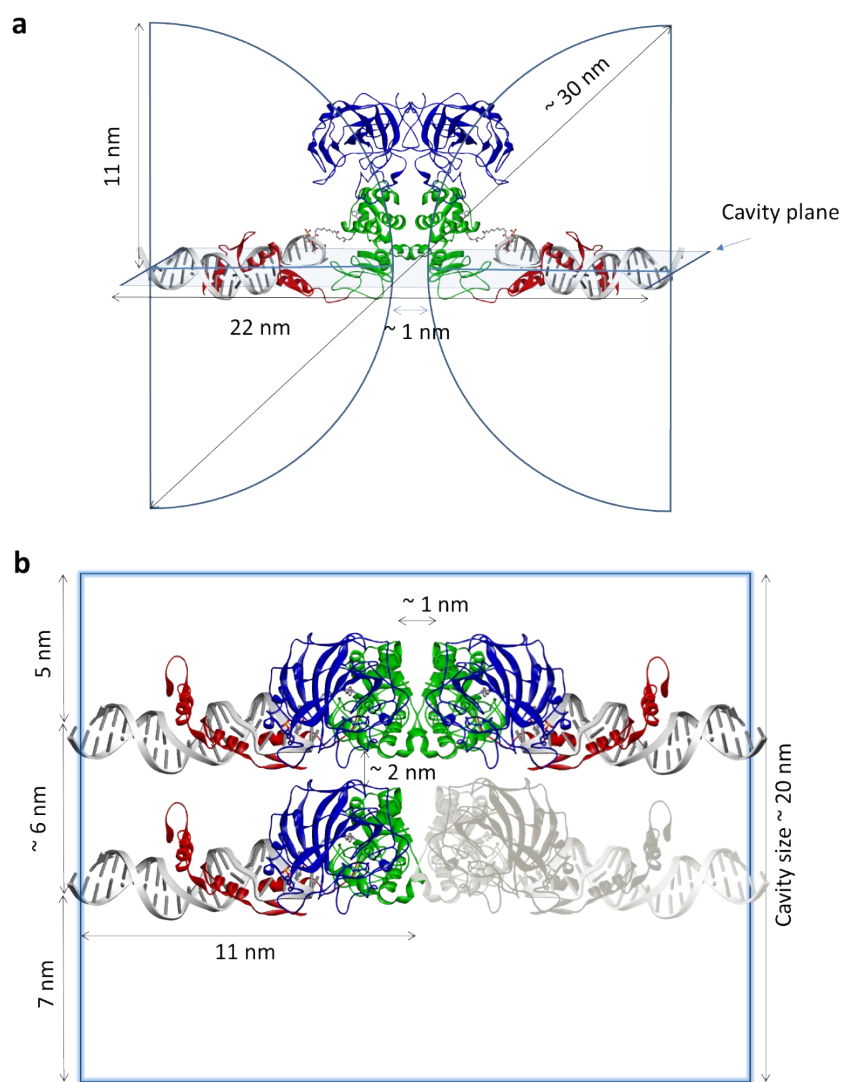


Figure S5. Illustrations show details of the distance of ZS-CA assembled in the central cavity of Ori-P. (a) A front view shows the distance from the inner edge of cavity to the outermost side of protein ZS-CA (~ 11 nm), the cavity size (22 nm), the possible distance of two ZS-CA molecules (~ 30 nm) and the distance of two ZS-CA molecules aligned in the cavity plane (~ 1 nm). The half-circles indicate the possible movement space of enzyme. (b) A top view illustrates four molecules of ZS-CA in the central cavity of Ori-P. One of the four ZS-CAs is colored in grey for better visualization. The models for ZS-CA and ODN-ZF-BG were constructed using Discovery Studio (version 3.1, Accelrys Inc.); based on the crystal structures of the zif268-DNA complex (PDB ID: 1ZAA; colored in red), SNAP tag (PDB ID: 3KZY; colored in green), and human carbonic anhydrase II (PDB ID: 2VVB; colored in blue).

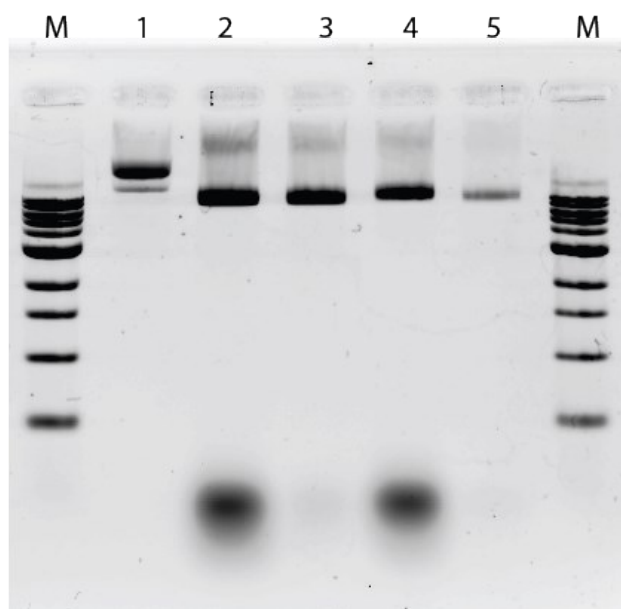


Figure S6. Agarose gel electrophoresis of the DNA scaffold before and after the purification. The gel was stained with ethidium bromide (EtBr) and visualized by using Molecular Imager FX pro (BioRad). Lane M: 1k bp DNA ladder, lane 1: 20 nM M13mp18 single strand, lane 2: Ori-D (20 nM before purification), lane 3: Ori-D after purification by size exclusion chromatography using 500 μ L volume of Sephacryl S-400 in Ultrafree-MC-DV column, lane 4: Ori-D (13.3 nM) incubated with ZS-CA (200 nM) in a buffer (pH 8.0) containing 40 mM Tris-HCl, 20 mM acetic acid, 12.5 mM $MgCl_2$, 1 μ M $ZnCl_2$, 0.001% Tween-20, 5 mM β -mercaptoethanol and of staple strands mixture for DNA scaffold (125 nM, without the staple strands with binding sites for ZS-CA); lane 5: sample in lane 4 after the purification by size exclusion chromatography. The samples were run on a 0.8% agarose gel ($0.5 \times TB$) with the following conditions: $0.5 \times TB$ buffer, 50 V for 2 h at 4 $^{\circ}C$.

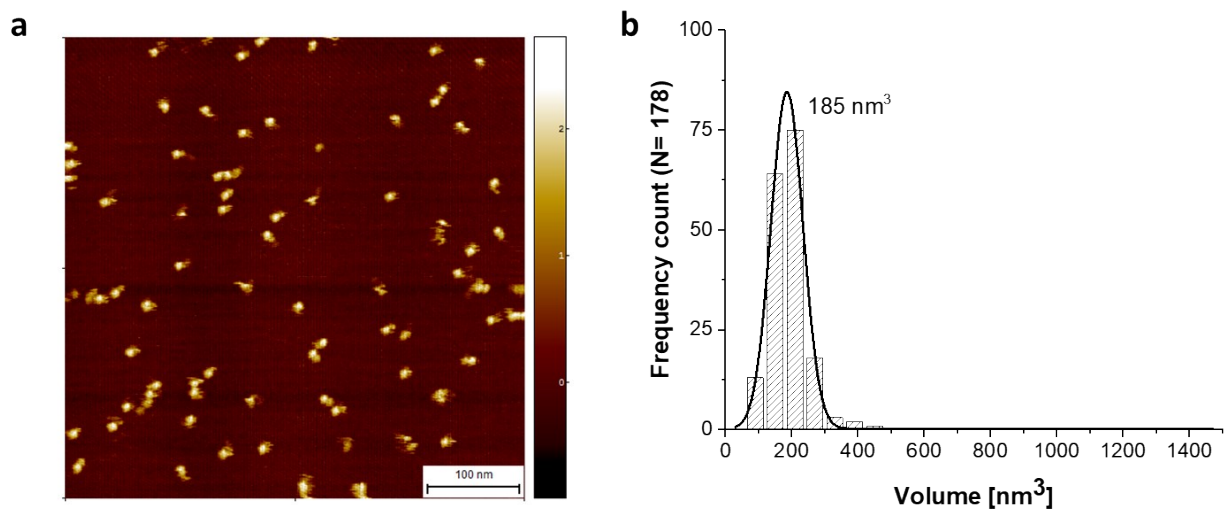


Figure S7. (a) AFM image of ZS-CA on a mica surface. (b) Analysis of the volume of ZS-CA. A solution containing 10 nM ZS-CA was applied directly on a freshly cleaved mica surface, incubated for 30 second then rinsed off with a buffer (pH 8.0) containing 40 mM Tris-HCl, 20 mM acetic acid, 12.5 mM MgCl₂. AFM image was taken in the same buffer.

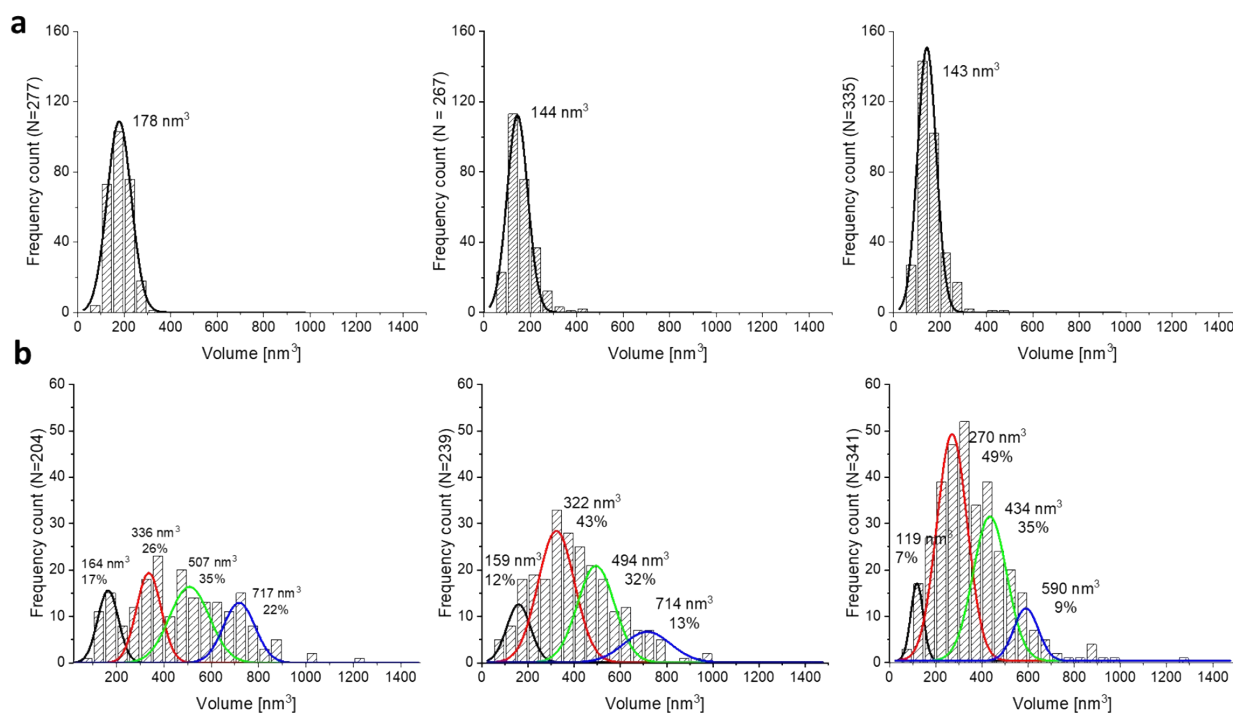


Figure S8. Analyses of the volumes of ZS-CA assembled on DNA scaffold for three independent experiments. (a) In the case of Ori-D, single ZS-CA revealed an average volume of 178 nm³, 144 nm³ and 143 nm³, respectively (from left to right). In these cases, the percentages of DNA cavities containing specifically assembled ZS-CA were determined from AFM images as 76%, 75%, 79%, respectively. Thus, the numbers of ZS-CA molecules bound to Ori D were calculated as 3.0, 3.0 and 3.2, respectively and the average of 3.1 molecules of ZS-CA on one Ori-D was used for the following experiments. (b) The volume of ZS-CA on Ori P with the respective volumes for one (black line), two (red line), three (green line) and four (blue line) molecules were estimated by fitting.² The percentages of specific ZS-CA loaded DNA cavities were determined from AFM images as 98%, 100%, 99%, respectively. In average, numbers of ZS-CA bound to Ori-P were calculated as 2.6, 2.5 and 2.5, respectively and 2.6 molecules of ZS-CA on one Ori-P was used for the following experiments.

In Figure 2b, the volume of ZS-CA in the dispersed state (Ori-D) distributed as a single peak with the most frequent value being $163 \pm 48 \text{ nm}^3$ ($n = 558$) (*left image*). This was in good agreement with the volume of ZS-CA measured on a mica surface ($185 \pm 97 \text{ nm}^3$, Figure S7). In the packed state (Ori-P), cavities occupied with one, two, three, and four ZS-CA molecules were estimated to represent 15, 33, 32, and 20% of the cases ($n = 207$), respectively (Figure 2b, *right*). The steric hindrance in the central cavity of Ori-P likely made ZS-CA less accessible to these binding sites than Ori-D with a single binding site per cavity.

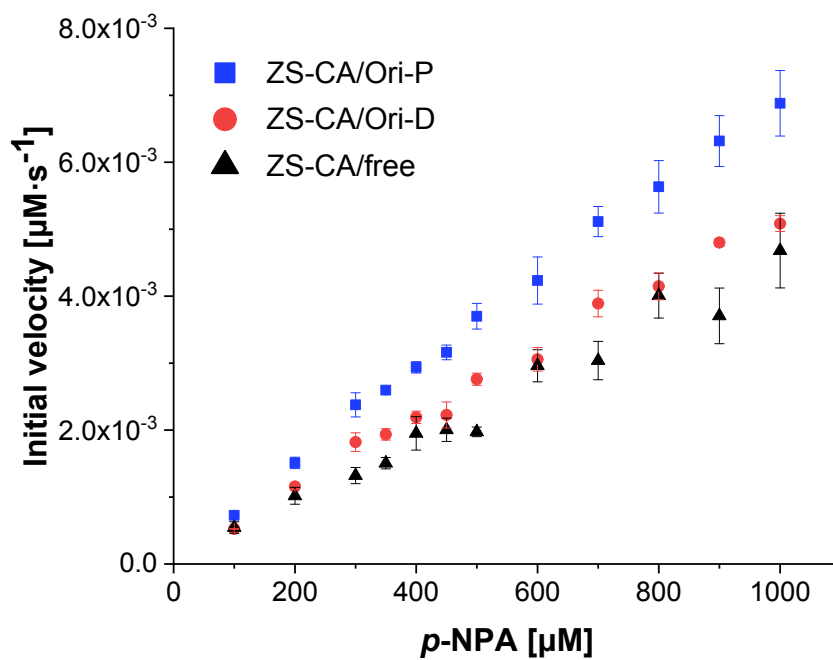


Figure S9. Plots of initial velocities of ZS-CA assembled on DNA scaffold against $p\text{-NPA}$ concentrations ranging from 0.1 mM to 1 mM. The reactions were carried out with 4 nM ZS-CA, 0.1 to 1 mM $p\text{-NPA}$ in a buffer (pH 7.6) containing 50 mM HEPES, 12.5 mM MgCl_2 , 1% acetonitrile, 1 μM ZnCl_2 and 0.001% Tween 20 at 25 °C. Error bars represent the mean \pm SD of three independent experiments.

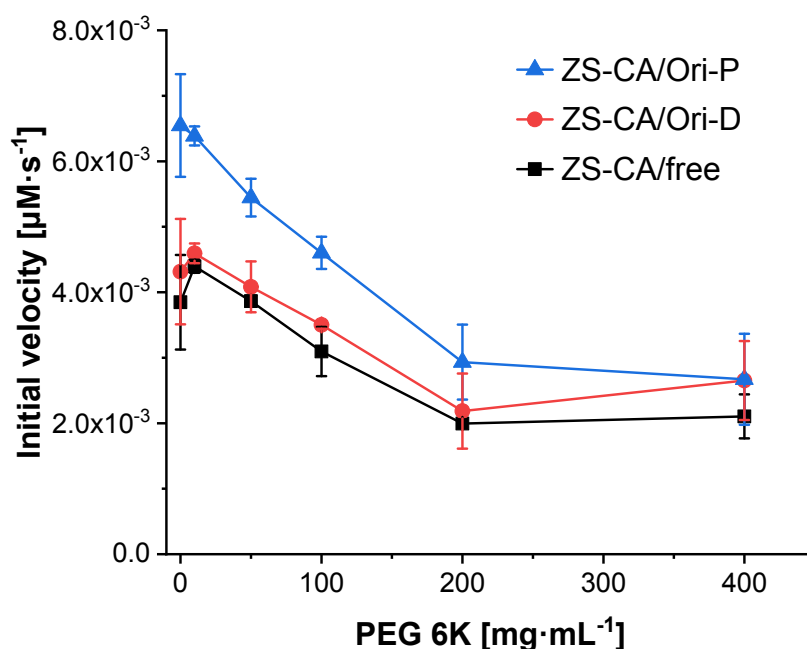


Figure S10. Initial velocity of the esterase reaction by ZS-CA in the presence of macromolecular crowding reagent PEG 6K. Increasing the concentration of PEG 6K decreased the reaction rate of enzyme ZS-CA in free solution (black line), assembled on Ori-D (red line) and on Ori-P (blue line). In all cases, the initial velocity of ZS-CA gradually decreased as PEG 6K concentration rose to 200 mg/mL. From these results, we conclude that acceleration of the ZS-CA esterase reaction in the packed state was not caused by the effect of macromolecular crowding reagents on protein stability. Reactions were carried out with 4 nM ZS-CA (in the bulk solution and in the complex with DNA scaffold), 1 mM *p*-NPA in a buffer (pH 7.6) containing 50 mM HEPES, 12.5 mM MgCl₂, 1% acetonitrile, 1 μM ZnCl₂ and 0.001% Tween 20 at 25 °C. Error bars represent the mean ± SD of three independent experiments.

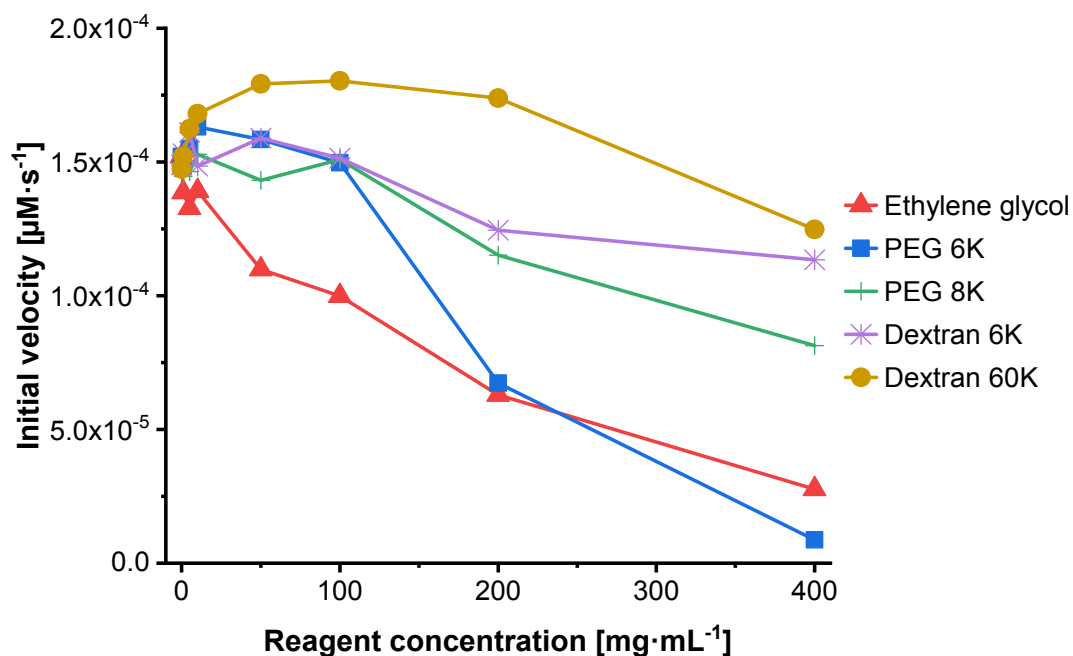


Figure S11. Effects of macromolecule crowding reagents at different concentrations on the initial velocity of the esterase reaction by ZS-CA in the presence of macromolecular crowding reagents, dextran 6K (stars), dextran 60K (filled circle), PEG 6K (filled rectangles), PEG 8K (crosses) and ethylene glycol (filled triangles). Increasing the concentration of macromolecular crowding reagents decreased the reaction rate of enzyme ZS-CA. Reactions were carried out with 50 nM ZS-CA, 1 mM *p*-NPA in a buffer (pH 7.6) containing 50 mM HEPES, 12.5 mM MgCl₂, 1% acetonitrile, 1 μM ZnCl₂ and 0.001% Tween 20 at 25 °C.

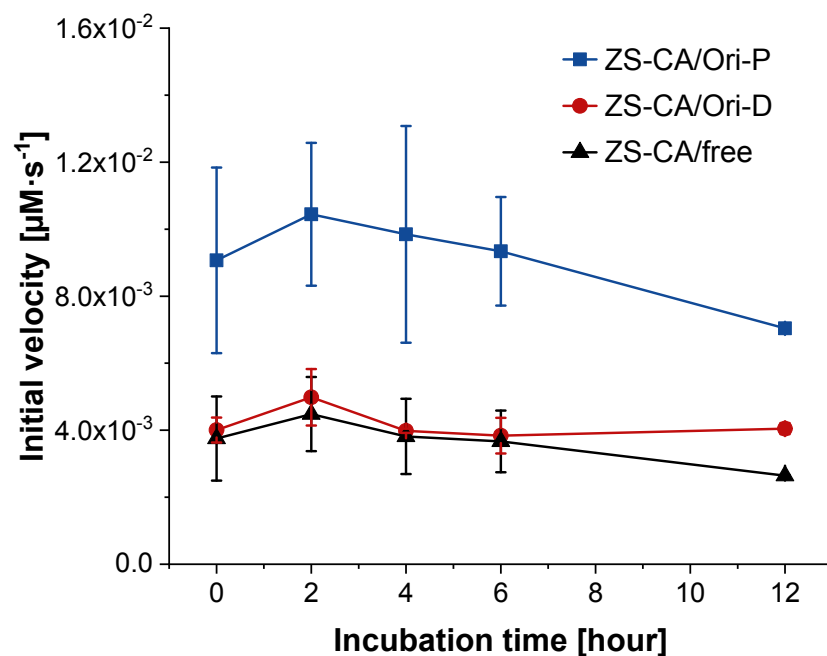


Figure S12. Plots of the initial velocities of ZS-CA against the time of incubation at 25 °C. ZS-CA showed the same thermal stability either in free solution or in the assembly on DNA scaffold (Ori-P or Ori-D) at 25 °C for 12 h. After the reaction of ZS-CA with Ori-D or Ori-P, the reaction mixture was subjected to size exclusion chromatography (500 μL volume of Sephacryl S400 in Ultrafree-MC-DV column) to remove the unbound enzyme. The sample was incubated at 25 °C for 2, 4, 6 and 12 h before measuring the activity. The free ZS-CA with the same concentration (4 nM) was used as a control experiment. Each reaction contained 4 nM ZS-CA (in bulk solution and in the complex with DNA scaffold), 1 mM *p*-NPA in a buffer (pH 7.6) containing 50 mM HEPES, 12.5 mM MgCl_2 , 1% acetonitrile, 1 μM ZnCl_2 and 0.001% tween 20 at 25 °C. Error bars represent the mean \pm SD of three independent experiments.

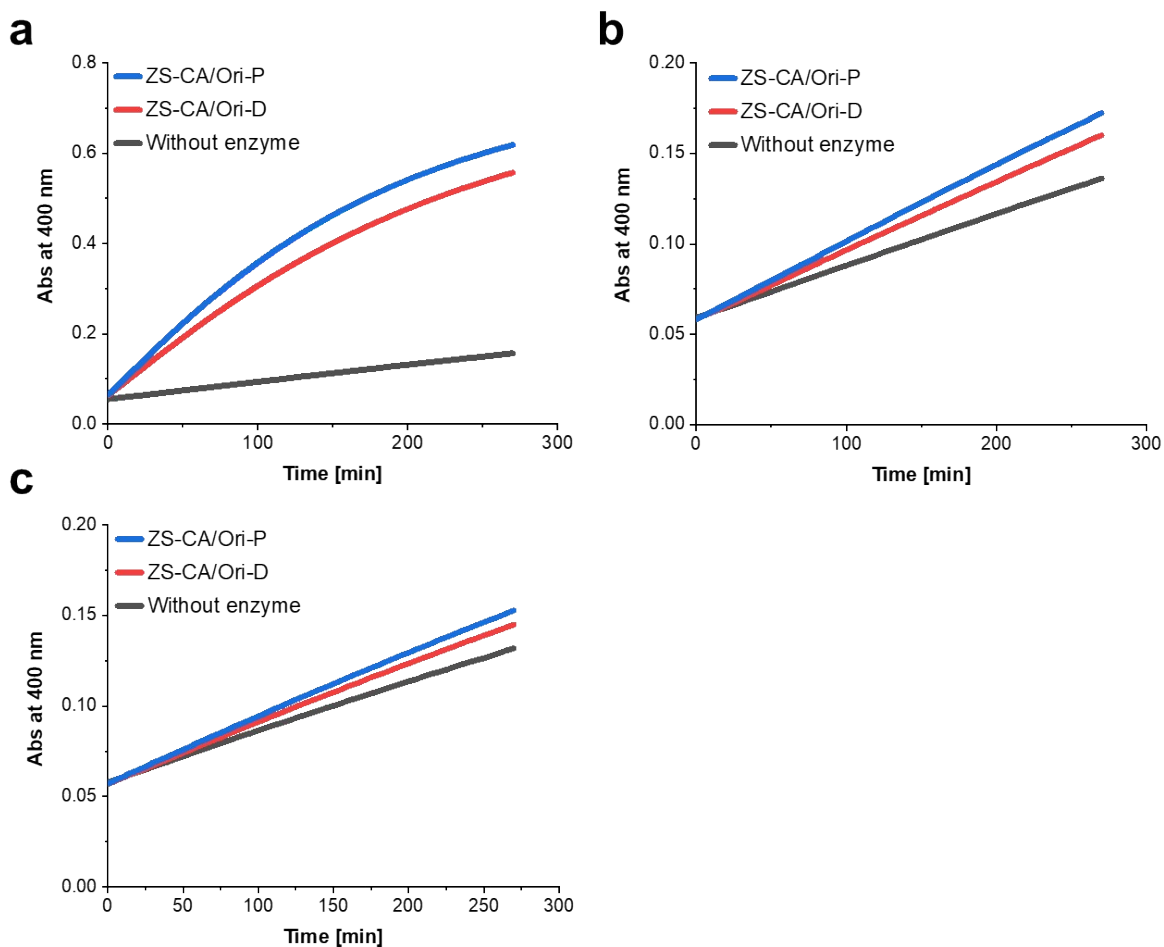


Figure S13. Esterase reactions of ZS-CA (23 nM) on DNA scaffold with 0.1 mM of *p*-NPA (a), *p*-NPB (b) and *p*-NPV (c) were monitored at 400 nm. The reactions were carried out in a buffer (pH 7.6) containing 50 mM HEPES, 12.5 mM MgCl₂, 5% acetonitrile, 1 μM ZnCl₂ and 0.001% Tween 20 at 25 °C. The initial velocities were calculated from the first 30 min (for *p*-NPA) and 200 min (for *p*-NPB and *p*-NPV) of reaction because the reactions of ZS-CA to *p*-NPB and *p*-NPV proceeded much slower than that to *p*-NPA.³ The enhancement in reaction rate of ZS-CA/Ori-P over that of ZS-CA/Ori-D was shown in Figure 4b for each substrate.

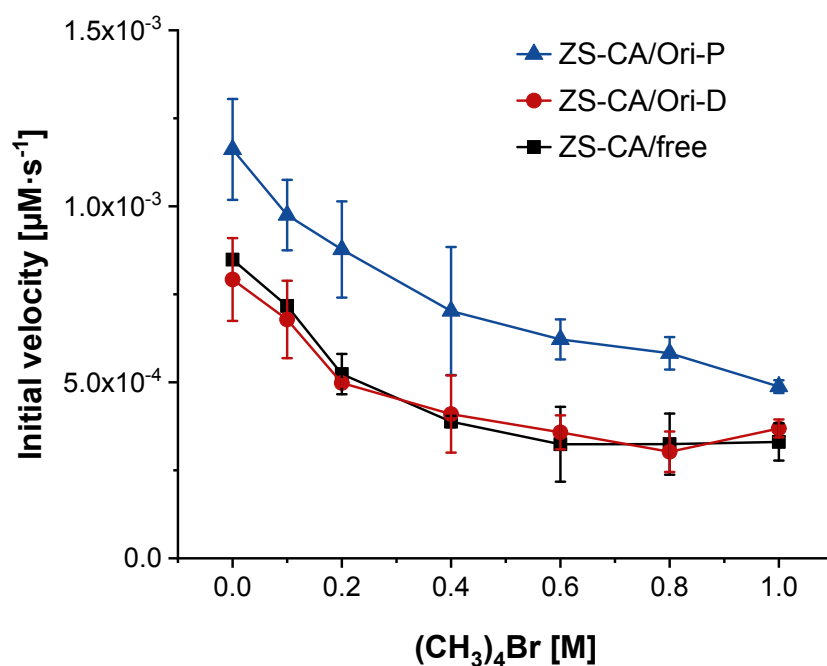


Figure S14. Effect of tetramethyl ammonium bromide (CH₃)₄NBr on the reaction rate of ZS-CA assembled on DNA scaffold (Ori-D and Ori-P) and free ZS-CA. Beside bromide ion being a non-competitive inhibitor of carbonic anhydrase,⁴ the choice of tetramethyl ammonium bromide (CH₃)₄NBr and sodium bromide NaBr (Figure 4c) was followed the discussion in "Effect of Salt Addition", for the addition of the weakly hydrated bromide ion might decrease the water-entropy effect in the system. Reactions (100 μL) were carried out with 5.5 nM ZS-CA in a buffer (pH 7.6) containing 50 mM HEPES buffer, 12.5 mM MgCl₂, 1% acetonitrile, 1 μM ZnCl₂ and 0.001% Tween20 and 0.1 mM substrate *p*-NPA. Error bars represent the mean ± SD of three independent experiments.

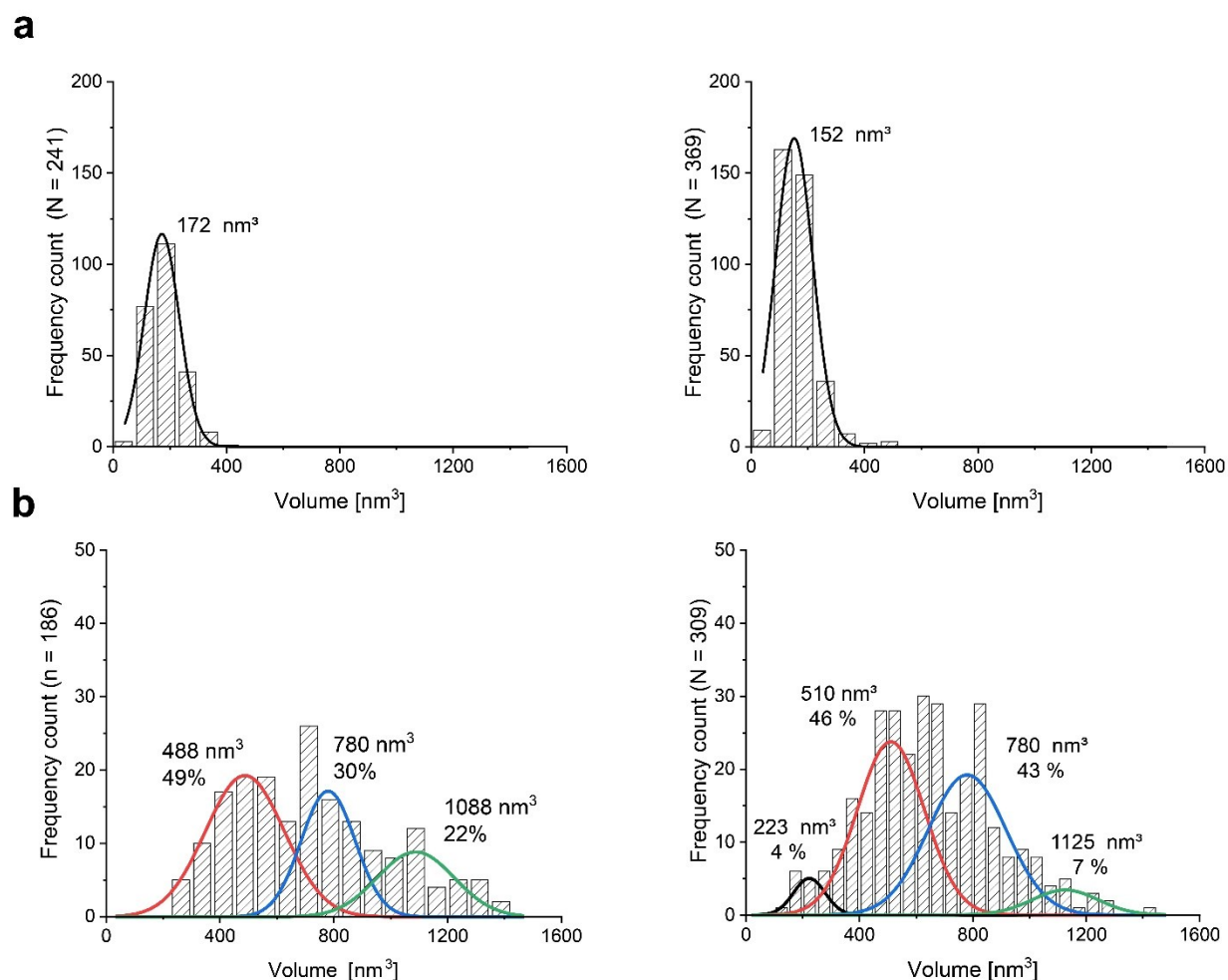


Figure S15. Analyses of the volumes of ZS-XR assembled on DNA scaffold for two independent experiments. (a) For assembly on Ori-D, ZS-XR showed an average volume of 172 nm³ (left) and 152 nm³ (right). The occupancies of ZS-XR on Ori-D were counted from AFM images as 82% for both cases. The numbers of ZS-XR molecules bound to Ori-D were calculated as 3.2. (b) The volume of ZS-XR on Ori-P with the respective volumes for one (black line), two (red line), three (green line) and four (blue line) molecules were estimated by fitting.² The occupancies of ZS-XR on DNA scaffold were determined from AFM images as 100%, 99%, respectively. In average, numbers of ZS-XR bound to Ori-P were calculated as 2.8 and 2.6, respectively and 2.7 molecules of ZS-XR on one Ori-P was used for the further experiments.

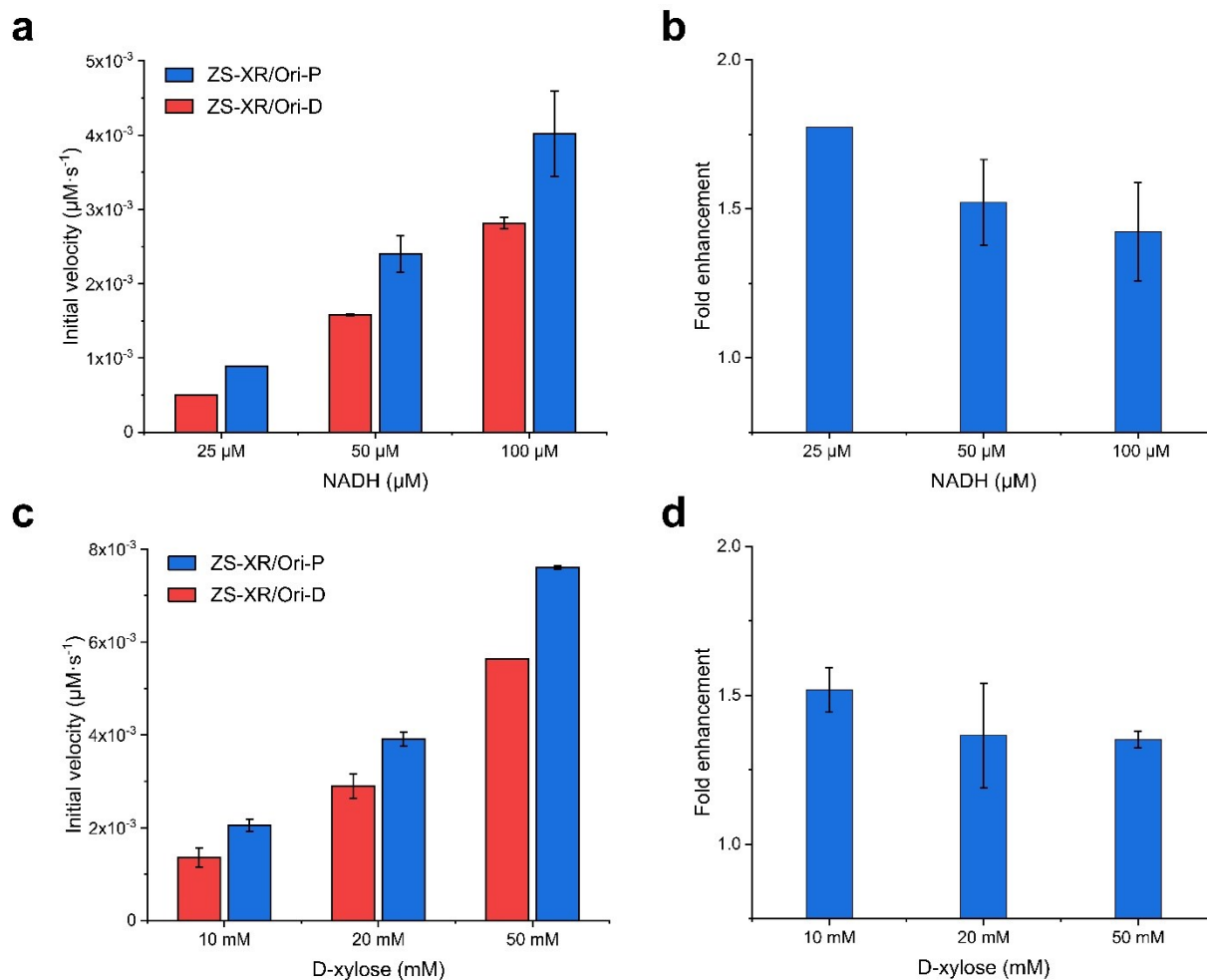


Figure S16. Activity of ZS-XR on DNA scaffold at the low substrate concentrations. (a) The initial reaction velocities of ZS/XR on Ori-D and Ori-P were represented with the NADH concentration ranged from 25 μM to 100 μM and the D-xylose concentration fixing at 5 mM. The ratio for the initial reaction velocity of ZS-XR/Ori-P over that of ZS-XR/Ori-D was represented as ‘fold enhancement’ in (b). (c, d) The initial reaction velocities of ZS/XR on Ori-D and Ori-P were represented with the D-xylose concentration ranged from 10 mM to 50 mM and the NADH concentration fixed to 25 μM . Reactions were carried out with 13 nM ZS-XR on DNA scaffold in a buffer (pH 6.8) containing 50 mM HEPES, 0.1 M NaCl, 12.5 mM MgCl_2 , 1 μM ZnCl_2 , 0.001% Tween20. Error bars represent the mean \pm SD of two independent experiments.

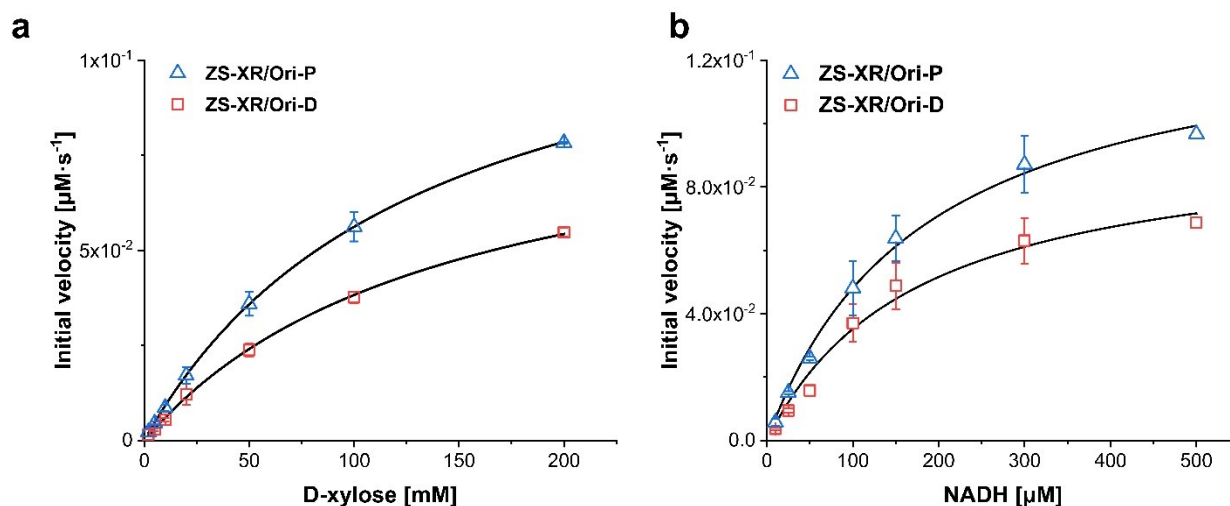


Figure S17. Plots of initial velocities of ZS-XR on DNA scaffold for D-xylose (a) and NADH (b) concentrations. The reaction was initiated by the addition of ZS-XR/Ori-P or ZS-XR/Ori-D (14 nM) to the reaction mixture of (a) 300 μM NADH and the increasing concentration of D-xylose and (b) 200 mM D-xylose and the increasing concentration of NADH in a buffer (pH 6.8) containing 50 mM HEPES, 0.1 M NaCl, 12.5 mM MgCl_2 , 0.001 μM ZnCl_2 , 0.001% Tween20. Error bars represent the mean \pm SD of two independent experiments.

The K_m and k_{cat} values for NADH calculated from the Michealis-Menten kinetic equation were 0.23 ± 0.01 mM and 0.16 ± 0.02 $\mu\text{M}\cdot\text{s}^{-1}$ for packed state and 0.24 ± 0.02 mM and 8.2 ± 1.1 s^{-1} for dispersed state, respectively. Likewise, the K_m and k_{cat} values for D-xylose were determined as 142 ± 40 mM and 9.6 ± 1 s^{-1} for packed state and 157 ± 35 mM and 7 ± 0.6 s^{-1} for dispersed state, respectively.

SUPPLEMENTARY REFERENCES

1. Kim, D. N.; Kilchherr, F.; Dietz, H.; Bathe, M.; Quantitative prediction of 3D solution shape and flexibility of nucleic acid nanostructures. *Nucleic Acids Res.* **2012** *40*, 2862–2868.
2. Nakata, E.; Dinh, H.; Ngo, T. A.; Saimura, M.; Morii, T. A Modular Zinc Finger Adaptor Accelerates the Covalent Linkage of Proteins at Specific Locations on DNA Nanoscaffolds. *Chem. Commun.* **2015**, *51*, 1016–1019.
3. Höst, G.; Mårtensson, L. G.; Jonsson, B. H. Redesign of Human Carbonic Anhydrase II for Increased Esterase Activity and Specificity towards Esters with Long Acyl Chains. *Biochim. Biophys. Acta, Proteins Proteomics* **2006**, *1764*, 1601–1606.
4. De Simone, G.; Supuran, C. T. (In)Organic Anions as Carbonic Anhydrase Inhibitors. *J. Inorg. Biochem.* **2012**, *111*, 117–129.